Excitation of surface plasmons at a SiO_2/Ag interface by silicon quantum dots: Experiment and theory

J. Kalkman,[1,*] H. Gersen,[2] L. Kuipers,[1,2] and A. Polman[1]

[1]*Center for Nanophotonics, FOM Institute for Atomic and Molecular Physics, Kruislaan 407, 1098 SJ Amsterdam, The Netherlands*

[2]*Applied Optics Group, University of Twente, P.O. Box 217, 7500 AE Enschede, The Netherlands*

(Received 15 April 2005; published 10 February 2006)

The excitation of surface plasmons (SPs) by optically excited silicon quantum dots (QDs) located near a Ag interface is studied both experimentally and theoretically for different QD-interface separations. The Si QDs are formed in the near-surface region of an SiO_2 substrate by Si ion implantation and thermal annealing. Photoluminescence decay-rate distributions, as derived from an inverse Laplace transform of the measured decay trace, are determined for samples with and without a Ag cover layer. For the smallest, investigated Si-QDs-to-interface distance of 44 nm the average decay rate at $\lambda = 750$ nm is enhanced by 80% due to the proximity of the Ag-glass interface, with respect to an air-glass interface. Calculations based on a classical dipole oscillator model show that the observed decay rate enhancement is mainly due to the excitation of surface plasmons that are on the SiO_2/Ag interface. By comparing the model calculations to the experimental data, it is determined that Si QDs have a very high internal emission quantum efficiency of $(77 \pm 17)\%$. At this distance they can excite surface plasmons at a rate of $(1.1 \pm 0.2) \times 10^4$ s^{-1}. From the model it is also predicted that by using thin metal films the excitation of surface plasmons by Si QDs can be further enhanced. Si QDs are found to preferentially excite symmetric thin-film surface plasmons.

DOI: 10.1103/PhysRevB.73.075317 PACS number(s): 73.21.La, 42.70.Ce, 73.20.Mf, 78.55.−m

I. INTRODUCTION

Silicon quantum dots (QDs) are crystalline clusters of 100–10 000 Si atoms that show quantum-confined luminescence at wavelengths in the visible or near infrared. Several microscale and nanoscale optoelectronic technologies based on Si QDs have been developed. Si-QD-based light-emitting diodes have been demonstrated,[1,2] as well as nonvolatile memory devices based on charge storage in Si QDs.[3] Also it has been suggested that optical gain from Si QDs may lead to the fabrication of a Si-based laser[4] (i.e., fully compatible with Si integrated-circuit manufacturing). The use of Si QDs in many of these optoelectronic devices requires precise control over their luminescence properties in often quite complex optical geometries. As first suggested by Purcell in 1946,[5] the spontaneous emission rate of an emitter not only depends on the electronic transition probability, but also on its dielectric surrounding. In dielectrics this is described by the local optical density of states (DOS).[6] In the most simple dielectric environment, a single dielectric interface, the DOS varies with the distance from the interface, which can result in a modification of the spontaneous emission rate for an optical emitter near the interface.[7,8] For an optical emitter near a metal, additional decay processes can occur, such as surface plasmon (SP) or lossy surface wave excitation that modify the spontaneous emission.[9–12]

In this paper we study the coupling between Si QDs embedded in SiO_2 and a Ag film. We measure the decay-rate distribution of the Si QDs. By varying the distance between the Si QDs and the Ag we demonstrate that Si QDs show an increased average decay rate that is mainly due to the excitation of SPs. By comparing our experimental results to model calculations, we determine the excitation rate of the SPs. As we will discuss, excitation of SPs that are subsequently coupled out into the far field can lead to an increased radiative decay and greater emission efficiency of Si QDs. We describe various possible ways to enhance the coupling of Si QDs to SPs to influence these effects further. Moreover, we determined the internal emission quantum efficiency (QE) of optically excited Si QDs and find that it is near unity.

II. EXPERIMENT

We create optically active Si QDs in SiO_2 near a Ag surface in the following way. The near-surface region of suprasil quartz slides (Heraeus) is implanted with Si^+ ions at energies of 28, 130, 267, or 400 keV. Monte Carlo calculations using the TRIM program[13] were performed to determine the projected range (R_p) and straggle (σ) of the Gaussian depth distribution of the implanted ions for the four implantation energies; see Table I. The implanted ion fluences, also listed in Table I, were chosen such that the peak Si concentration was approximately 5 at. %. After implantation, the samples were annealed for 10 min at 1100 °C under an Ar flow to nucleate the QDs. Subsequently, the samples were annealed for 30 min at 800 °C under a flow of forming gas (H_2:N_2

TABLE I. Implantation conditions for the four Si-implanted samples, the projected range (R_p) and straggle (σ) were calculated.

Energy (keV)	R_p (nm)	σ (nm)	Fluence (Si/cm^2)
28	44	18	1.4×10^{16}
130	193	59	3.7×10^{16}
267	401	99	7.2×10^{16}
400	593	132	9.3×10^{16}

 ©2006 The American Physical Society

=1:9), a process that is known to increase the luminescence yield of the Si QDs, due to passivation of quench sites.[14] Finally, an optically thick (225 nm) Ag layer was deposited on one part of the sample using sputtering of a pure Ag target in an Ar ambient at a pressure of 5 μbar. The deposition rate was 2.5 nm/s. The dielectric constant of the Ag was measured by spectroscopic ellipsometry in the wavelength range of 300–1700 nm. Photoluminescence (PL) spectroscopy was performed at room temperature using an Ar-ion laser operating at 488 nm. The laser intensity, modulated at 667 Hz with an acousto-optical modulator, was incident through the transparent backside of the sample. The PL was collected from the back using an $f=10$ cm lens; guided through a long-pass filter ($\lambda > 524$ nm) and dispersed using a 480-mm focal-length monochromator, set to a resolution of 3 nm. An AgOCs photomultiplier recorded the collected and dispersed PL intensity. PL decay measurements were taken with a multichannel photon counting system. The system time resolution was 100 ns. To determine the influence of the metal on the emission of the Si QDs, PL spectra and decay rates were always compared for two sections of the same sample: one part covered with Ag and one part not covered, eliminating unwanted differences due to the different implantation conditions. More importantly, it allows an unambiguous and model-independent determination of the change in the decay due to the presence of the metal-dielectric interface.

III. RESULTS AND DISCUSSION

A. Quantitative analysis of stretched-exponential decay

For a quantitative comparison of Si QD PL decay rate measurements it is important to realize that the time decay of the Si QD emission at a given detection wavelength is not described by a single decay rate, but rather a distribution of decay rates.[15–17] This distribution reflects a variation in the Si QD emission characteristics, which can be caused by several factors.

(1) The large linewidth of the emission of individual Si QDs at room temperature[18,19] leads to a distribution of decay rates at a given emission wavelength.

(2) Variations in the amount of interaction between Si QDs cause a distribution of decay rates. The interaction, which can cause quenching, is sensitive to variations in the nearest-neighbor distance. The distribution of nearest-neighbor distances is determined by small-scale inhomogeneities due to the nature of the nucleation and growth process of the Si QDs and large-scale variations in Si concentration (as for the Gaussian implantation depth profiles used here).[16,20]

(3) Si QDs with identical emission wavelengths may have varying degrees of surface passivation and thus different nonradiative decay rates.[21]

(4) Si QDs with identical emission wavelengths may have slightly different geometrical shapes and/or strains[22] and thus a different decay rate.

(5) Charge trapping at defect states causes intermittent Si QD emission (blinking) and thus leads to a variation in decay rate.[2,23]

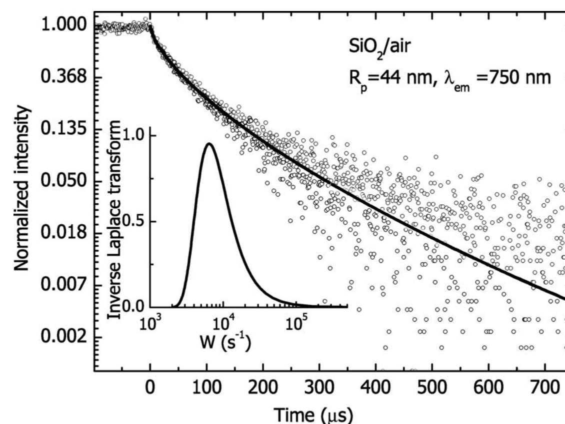

FIG. 1. PL decay measured at $\lambda=750$ nm for the shallowest Si implant ($R_p=44$ nm) on a part of the sample not covered with Ag. At $t=0$ the laser is switched off and a stretched exponential PL decay can be observed. The solid line shows a stretched exponential fit of the data, which corresponds to the decay rate distribution shown in the inset.

(6) Pump power dependent decay processes can cause variations of the decay rate for Si QDs emitting at a fixed wavelength.[20,23]

(7) Identical Si QDs located at different positions in their photonic environment will experience a different decay rate due to spatial variations in both the local density of states and nonradiative processes, as will be discussed in this paper.

The combination of all, or some, of the above-mentioned effects result in a nonsingle exponential decay of the Si QD population. As an example of the nonsingle-exponential Si QD decay, Fig. 1 shows a Si QD PL decay trace measured at $\lambda=750$ nm for the 400 keV Si implanted sample. The decay curve was fitted with a four-parameter equation for a stretched exponential decay: $I=I_0+I_1\exp(-(t/\tau_{\mathrm{exp}})^{\beta})$, with offset ($I_0$), amplitude ($I_1$), lifetime ($\tau_{\mathrm{exp}}$), and stretchiness ($\beta$). An excellent agreement with the data was obtained as can be seen by the fit overlaying the data in Fig. 1. In the past, several methods have been applied to determine the distribution of decay rates underlying the stretched exponential function,[24,25] here we will use the method outlined by Lindsey and Patterson.[26] The stretched exponential decay can be described as the Laplace transform of $\rho(\tau)$, a lifetime distribution, in the following way:

$$e^{-(t/\tau_{\mathrm{exp}})^{\beta}} = \int_0^{\infty} e^{-t/\tau}\rho(\tau)d\tau. \tag{1}$$

Using substitutions: $s=t/\tau_{\mathrm{exp}}$, $x=\tau_{\mathrm{exp}}/\tau=W/W_{\mathrm{exp}}$, and $\lambda(x,\beta)=(\tau_{\mathrm{exp}}/x^2)\rho(\tau_{\mathrm{exp}}/x)$, and W the decay rate, the integral can be rewritten into a standard Laplace integral

$$e^{-s^{\beta}} = \int_0^{\infty} e^{-sx}\lambda(x,\beta)dx, \tag{2}$$

with $\lambda(x,\beta)$ the rate distribution. The function $\lambda(x,\beta)$ can be written analytically[27] as a series solution

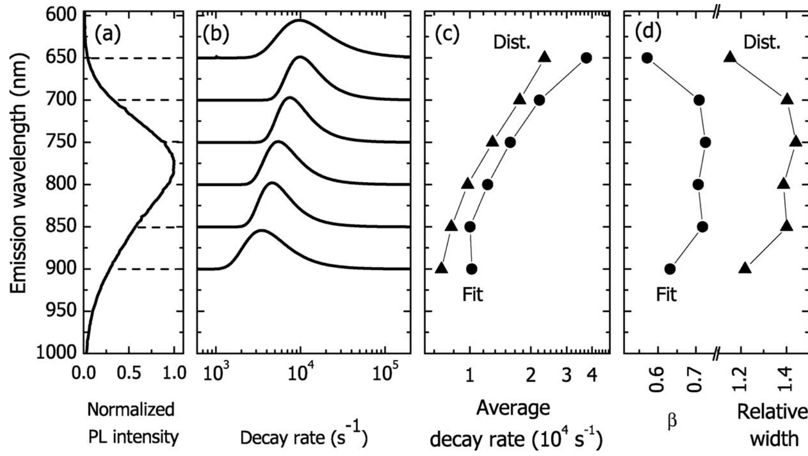

FIG. 2. (a) PL emission spectrum for the deepest (R_p=593 nm) Si implant, measured on the part of the sample not covered with Ag. (b) Decay rate distributions obtained from PL decay measurements, shifted vertically to the indicated wavelengths [dashed lines in (a)]. (c) Average decay rate obtained from the decay rate distribution (triangles) and decay rates obtained from the stretched-exponential fit (circles). (d) Inverse of the relative FWHM obtained from the decay rate distributions (triangles) and stretched-exponential fit parameter β (circles).

$$\lambda(x,\beta) = -\frac{1}{\pi}\sum_{k=0}^{\infty}\frac{(-1)^k}{k!}\sin(\pi\beta k)\frac{\Gamma(\beta k+1)}{x^{\beta k+1}}, \quad (3)$$

with Γ the gamma function. With $\tau_{\rm exp}$ and β obtained from the fit to the experimental data, $\lambda(x,\beta)$ was calculated over a range of x values. The domain of x was chosen such that $\lambda(x,\beta)$ was sufficiently small for both the largest and smallest x in the domain. In particular, we choose the lower boundary of the domain as the smallest x where convergence of Eq. (3) could still be reached. Outside the domain the function was assumed to be zero. The distribution $\lambda(x,\beta)$ obtained from the stretched-exponential fit of the PL decay trace in Fig. 1 is plotted in the inset. To verify the correctness of our procedure, the obtained distribution was then Laplace transformed to recalculate the decay trace. Perfect agreement with the stretched-exponential decay fit was obtained (identical drawn curves in Fig. 1). Since the first moment of the decay rate distribution is divergent,[26] an average decay rate cannot be calculated. However, since the average lifetime $\langle\tau\rangle$ can be calculated, we approximate the average decay rate by

$$\langle W\rangle \approx \langle\tau\rangle^{-1} = \frac{\beta}{\tau_{\rm exp}}\Gamma^{-1}(\beta^{-1}). \quad (4)$$

In the remainder of this paper, the thus defined average decay rate will be used to compare the decay rates of different samples.

To further explore the relation between the parameters of the stretched exponential function and the corresponding decay-rate distribution, we examine a characteristic Si QD emission spectrum for the sample with the deepest Si implant and not covered with Ag. Figure 2(a) shows the Si QD PL emission spectrum for the sample implanted with 400 keV Si. At various emission wavelengths (dotted horizontal lines) the PL decay was measured and fitted using a stretched-exponential decay. The rate distributions, obtained from the fits, are plotted in Fig. 2(b) for six different emission wavelengths. The rate distributions are shifted vertically to match with the dashed lines in Fig. 2(a) to indicate the emission wavelengths at which the PL decay was measured. It can be clearly seen that the rate distribution shifts to lower rates as the emission wavelength increases. This is attributed to a combined effect of a DOS effect that causes the decay rate to increase with frequency and a decreasing exciton recombination probability with increasing QD size.[28] From the rate distributions two quantities were calculated: the average decay rate and the inverse of the full width at half maximum (FWHM) normalized to the average decay rate $[1/(\langle\tau\rangle{\rm FWHM})]$. Figure 2(c) shows the average decay rates (triangles), again showing the decreasing trend with increasing emission wavelength. For comparison, the decay rates obtained from the stretched-exponential fit ($1/\tau_{\rm exp}$) are also plotted (circles). Both parameters follow a similar trend, although at slightly different absolute values, which is due to the way the width of the distribution affects the average decay rate. The decay rates are in the range of $(1-4)\times10^4$ s^{-1}, typical values for Si QDs made by ion-implantation.[16,29] Figure 2(d) shows the inverse of the relative width of the distributions (triangles), derived from the data in Fig. 2(b). For comparison, β values from the corresponding stretched-exponential fit are also shown (circles). The parameter β is in the range of 0.55–0.7, which are typical values for Si QDs made by ion implantation.[16] Both parameters in Fig. 2(d) show the same trend with wavelength, reflecting that a small value of β corresponds to a large distribution width, the typical characteristic of a stretched-exponential function.

B. Optical characterization

Figure 3(a) shows the normalized PL spectra for the samples with Si QDs located at four different depths from the interface for the sample in air (a) and covered with Ag (b). The spectra are shifted vertically to facilitate their comparison. The emission spectra are typical of quantum-confined emission from Si QDs. For large implantation depths the emission peaks at 775 nm (1.6 eV), which corresponds to a Si QD diameter of 3.8 nm.[30] The width of the emission spectrum is 290 meV (FWHM). Measurements on single Si QDs show a linewidth of 120–210 meV,[18] implying that the linewidth observed here is due to both the intrinsic Si QD emission spectrum width and inhomogeneous effects. While the spectrum of the three deepest implants peak at a similar wavelength, the spectrum from the Si QDs closest to the interface is significantly blueshifted. We attribute this shift, which reflects a smaller Si QD size, to a different

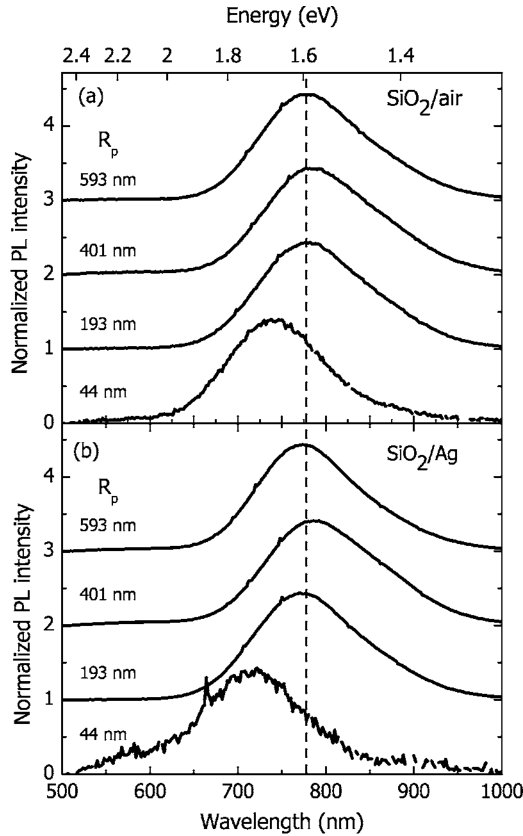

FIG. 3. Normalized Si QD emission spectra measured on the four Si implanted samples either in air (a) or covered with Ag (b). Spectra are shifted vertically for clarity. The peak depths (R_p) of the four Si-implants are indicated. In all samples Si QDs are excited with $\lambda=488$ nm laser light.

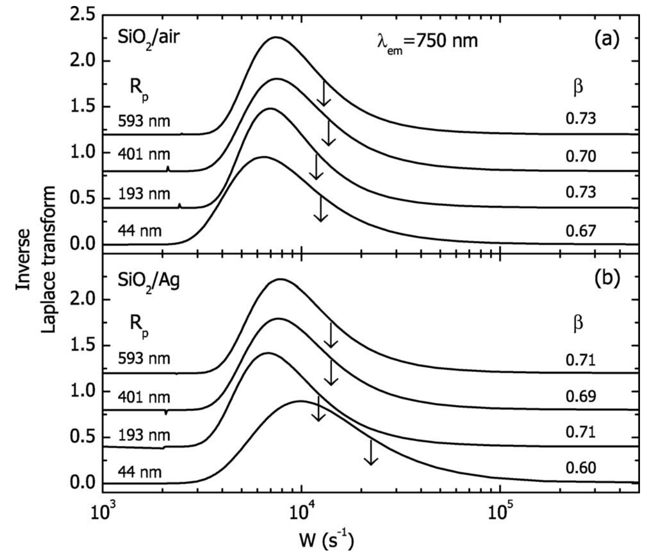

FIG. 4. PL decay rate distributions obtained from stretched-exponential PL decay traces measured at $\lambda=750$ nm for the four Si implants (depths R_p indicated). Data are shown for the sample in air (a) and covered with Ag (b) and are shifted vertically for clarity. Vertical arrows indicate the average decay rate and the β parameters of the corresponding stretched-exponential fit are also indicated. For the Si QD distribution closest to the Ag interface the decay rate is significantly increased.

Si QD nucleation and growth mechanism caused by the small width of the distribution or the proximity of the interface, which may lead to a different QD size distribution. PL spectra for the sample covered with Ag [Fig. 3(b)] show the same trend as for the sample in air, with a blueshift observed for the shallowest Si implant.

With the decay-rate distributions determined in a systematic way, as in Fig. 2, and by measuring the Si QD decay rate in the low pump power limit (where the decay rate is independent of pump power), the influence of the Ag layer on the PL decay rate of Si QDs in SiO_2 can be quantified by calculating and comparing the average decay rate for the two interfaces. Figure 4 shows the decay rate distributions for the four samples with different Si implantation depths. The rate distributions are calculated from the PL decay traces measured at a PL emission wavelength of 750 nm, both for the sample in air (a) and covered with Ag (b). The arrows indicate the average decay rates determined as described in Sec. III A. For the air-covered sections, the decay rate distributions have an average of $(1.2-1.4)\times 10^4$ s^{-1} and show no dependence on the depth. The same samples covered with Ag show a similar average decay rate for the three deepest Si implantations. However, for the shallowest Si implant the average decay rate near the Ag is significantly larger $(2.2\times 10^4$ s$^{-1})$ as compared to the decay rates found on the same sample but without the presence of the Ag. Note that on the logarithmic scale in Fig. 4 the effect of the Ag layer may appear relatively small, but with the analysis introduced above we can now clearly conclude that the presence of the Ag enhances the average PL decay rate of Si QDs for the shallowest implant. For this sample the average decay rate increases from $(1.25\pm 0.05)\times 10^4$ s^{-1} for the air-covered section to $(2.2\pm 0.2)\times 10^4$ s^{-1} for the Ag-covered section, an enhancement by a factor 1.8 ± 0.2. It is also clear from Fig. 4(b) that for the shallowest Si implant the presence of Ag increases the width of the decay rate distribution.

C. Modeling the Si QD decay

The decay rate of an oscillating dipole in a (metallo-) dielectric environment can be calculated using a classical model as developed by Ford and Weber.[31] In brief, the model calculates the decay rate of a dipole by determining the electric field at its position. The total electric field at the position of the dipole is the result of the dipolar field and the fields reflected from the dielectric surrounding of the dipole. To calculate these fields, the dipolar electric field is Fourier transformed into its spatial wave-vector components. The fields resulting from reflections at the interfaces are then calculated for each wave vector using the Fresnel reflection coefficients of the interface, which are determined using the dielectric constants as input parameters. After integration over the out-of-plane wave vectors the electric field at the position of the dipole is a function of normalized in-plane wave vector only ($k_\parallel/k_d$, with $k_d=n_d\ \omega/c$ the magnitude of the wave vector of a plane wave in the dielectric as determined by the optical frequency ω of the spontaneous emission and the refractive index n_d of the dielectric). By taking

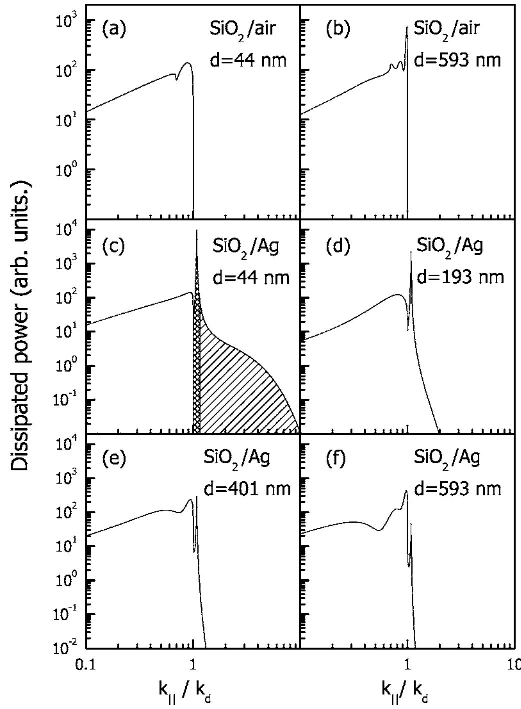

FIG. 5. Power dissipation as a function of in-plane wave vector for a randomly oriented dipole located near a SiO_2/air interface, emitting at $\lambda=750$ nm, for a distance of 44 nm (a) and 593 nm (b) to the interface. (c)–(f) The same calculation, but for a SiO_2/Ag interface and distances of 44, 193, 401, and 593 nm to the interface. The wave-vector region $k_{\|}/k_d \leqslant 1$ corresponds to spontaneous emission, $1 < k_{\|}/k_d \leqslant 1.158$ to SP excitation and $k_{\|}/k_d > 1.158$ to lossy surface wave excitation. The different wave-vector ranges are indicated in (c) with different fill patterns.

the imaginary part of the product of the electric field at the position of the dipole and the dipole moment, the power dissipation can be calculated at any normalized in-plane wave vector. Integrating the power dissipation over all in-plane wave vectors divided by the photon energy $\hbar\omega$ then yields the total decay rate of the dipole. In this analysis the parallel and perpendicular dipole orientations relative to the interface are treated separately. They are then averaged to obtain the decay rate for a randomly oriented dipole, as is the case for Si QDs in the amorphous SiO_2 host.

In our analysis we use the dielectric constants of Ag ($\varepsilon_{\mathrm{Ag}}=\varepsilon'_{\mathrm{Ag}}+i\varepsilon''_{\mathrm{Ag}}=-15+i0.86$) and SiO_2 ($\varepsilon_{\mathrm{SiO_2}}=2.1$) at $\lambda=750$ nm to calculate the power dissipation of a randomly oriented dipole as a function of normalized in-plane wave vector for a given distance from the interface. Figure 5(a) shows the result for a dipole at 44 nm from an SiO_2/air interface. This distance corresponds to the peak position of the shallowest Si implant. Power is dissipated for $k_{\|}/k_d \leqslant 1$ corresponding to spontaneous emission in the SiO_2 and air regions. In this wave-vector range $k_{\|} < k_d$ so that far-field plane waves with a real wave vector perpendicular to the interface are allowed. The small wiggle at $k_{\|}/k_d \sim 0.69$ is due to the difference in power dissipation for wave vectors in air ($k_{\|}/k_d < 0.69$) and SiO_2 ($k_{\|}/k_d < 1$). Figure 5(b) shows a similar calculation, but now for a dipole at 593 nm from the interface. Due to the larger distance interference wiggles are observed that are due to constructive or destructive interference of the reflected dipolar field, which either increases or decreases the dipole's power dissipation for a particular wave vector. The total power dissipation for the two depths, i.e., the integral over the power dissipation spectra in Figs. 5(a) and 5(b), is nearly identical. This is due to the relatively small reflection at the SiO_2/air interface. Figure 5(c) shows a similar calculation as for Fig. 5(a) (dipole located at 44 nm), but for the SiO_2/Ag interface. Again, power is dissipated for $k_{\|}/k_d \leqslant 1$, corresponding to spontaneous emission into the far field. However, in contrast to the case for the SiO_2/air interface, power is also dissipated for larger wave vectors ($k_{\|}/k_d > 1$). In this wave-vector range $k_{\|} > k_d$, so that the wave vector of the waves perpendicular to the interface must be fully imaginary. This leads to waves bound to the interface. First, a power dissipation resonance is observed for $k_{\|}/k_d = 1.078$, corresponding to the ratio $\sqrt{\varepsilon'_{\mathrm{Ag}}/(\varepsilon'_{\mathrm{Ag}}+\varepsilon_{\mathrm{SiO_2}})}$; the wave vector for a SP propagating along the SiO_2/Ag interface, normalized to the wave vector for a plane wave in SiO_2. The width of the resonance is determined by dissipation in the metal (represented by $\varepsilon''_{\mathrm{Ag}}$, the imaginary part of the dielectric constant for Ag), which is relatively small at this wavelength ($1/e$ SP intensity propagation length is ~ 8 μm). A considerable amount of power is contained in the SP resonance (note the log scale). At larger wave vectors power is dissipated to lossy surface waves:[31] loss processes such as electron-hole excitation and electron scattering in the Ag. Similar calculations are performed for dipoles spaced 193, 401, and 593 nm from the SiO_2/Ag interface, and are shown in Figs. 5(d)–5(f). The calculations show that the excitation rate of lossy surface waves decreases very rapidly as the distance increases. Also the excitation rate of SPs decreases, although less rapidly. Indeed, SP excitation is a near-field effect that, for optical wavelengths, is known to occur for distances up to ~ 100 nm, while the dissipation into lossy surface waves typically occurs on a 10 nm length scale. Note that the wiggles observed for $k_{\|}/k_d \leqslant 1$ are more pronounced in the Ag covered sample than for the sample in air [Figs. 5(a) and 5(b)], due to the larger reflectivity of the interface. The minima and maxima occur at different wave vectors than for the SiO_2/air interface, owing to the different phase shifts that occur upon reflection from either the SiO_2/Ag or the SiO_2/air interface.

Since the various ranges of normalized in-plane wave vector in Fig. 5 represent different decay channels, the decay rate of the dipole into these channels can be obtained by an integration of the dissipated power over the corresponding wave-vector range, indicated with different fill patterns in Fig. 5(c): spontaneous emission: $k_{\|}/k_d < 1$, surface plasmon excitation: $1 \leqslant k_{\|}/k_d < 2k_{\mathrm{SP}} - 1 = 1.158$,[32] and lossy surface wave excitation: $k_{\|}/k_d \geqslant 1.158$. For a distance of 44 nm and an emission wavelength of 750 nm the SP excitation rate is calculated using three different methods: the above-mentioned integration over the wave-vector range, a full Lorentzian fit of the SP resonance, and using an approximation for the Ag reflection coefficient;[31] all methods giving the same dissipated power. It should be noted that at wavelengths much closer to the SP resonance ($\lambda < 500$ nm) and at much shorter distances ($d < 10$ nm) from the interface the

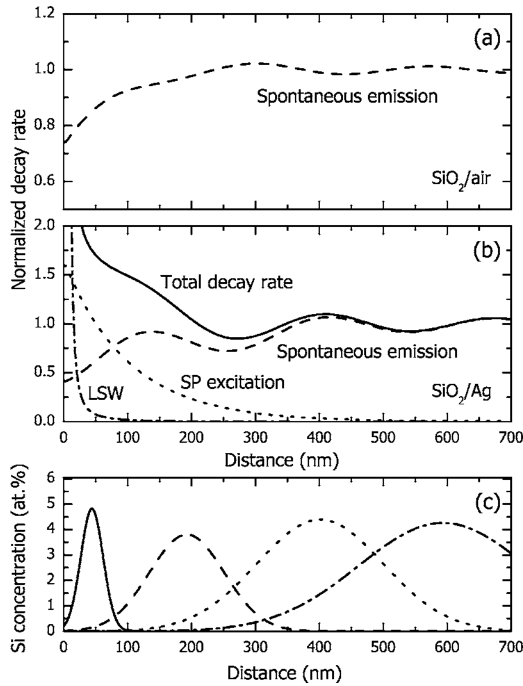

FIG. 6. Normalized decay rate as a function of distance from a SiO_2/air interface (a) and an SiO_2/Ag interface (b). For the SiO_2/Ag interface sample the total decay rate is divided into its three constituent parts: spontaneous emission, SP excitation, and lossy surface wave (LSW) excitation. In (c) the Si depth distributions are plotted for the four implants.

wave-vector integration range is not a valid approximation for the SP excitation rate calculation. The result of this integration procedure is shown in Fig. 6 for a range of dipole distances from the interface. Figure 6(a) shows the distance dependent decay rate for a dipole near the SiO_2/air interface. The rate is normalized to unity for large distances from the interface. As can be seen, close to the interface the normalized decay rate is significantly lower than for a dipole in the bulk of the material. We attribute the fact that this is not observed in the decay rate distributions shown in Fig. 4(a) to the blueshift of the Si QD PL emission. This blueshift, which is shown in Fig. 3(a), represents a smaller average QD size that leads, due to the large emission linewidth of individual Si QD, to an increase of the average Si QD decay rate, which may thus compensate for the decrease of the decay rate by the DOS. The decay rate shows oscillating behavior as a function of distance, due to the interference of reflected waves with the direct dipole field that either increases or decreases the dipole's dissipation rate. A similar effect was reported earlier in Refs. 7 and 33 for the case of 1.5 μm emission of Er^{3+} ions near a SiO_2/air interface. Figure 6(b) shows the calculated decay rates for the dipole in proximity to the SiO_2/Ag interface. The contributions of spontaneous emission, SP excitation, and lossy surface wave excitation are plotted separately; the total decay rate is also shown. The spontaneous emission rate shows oscillating behavior; when compared to the data in Fig. 6(a) the oscillation has a larger amplitude, which is due to the larger reflectivity of the interface. The maxima and minima occur at different depths for the SiO_2/Ag interface than for the SiO_2/air interface, due to a different phase change upon reflection at the SiO_2/Ag interface. The SP excitation rate decreases exponentially as a function of distance as would be expected from the exponentially decreasing field amplitude of the SP in the dielectric.[31] Lossy surface wave excitation occurs only at very short distances (<50 nm) from the interface and shows a d^{-3} dependence. This is in agreement with the distance dependence expected for an r^{-6} dipole-dipole interaction, integrated over a planar sheet of dipoles.

To compare the various decay processes for the four different Si implants, the depth profiles for the four Si implants are shown in Fig. 6(c). It is clear that for the three deepest Si implants the decay is dominated by spontaneous emission. The normalized decay rates for the SiO_2/air and SiO_2/Ag interface integrated over the depth distributions for these implants are close to unity. Indeed, these samples with and without Ag show similar PL decay rates, as can be seen in Figs. 4(a) and 4(b). Next, we analyze the decay for the shallowest Si implant that peaks at 44 nm. At the peak the normalized decay rates are 0.848 ± 0.002 and 1.75 ± 0.08 for the SiO_2/air and SiO_2/Ag interface, respectively. The error bars are calculated by taking into account the straggle of the Si depth profile and assuming a symmetric spread of Si QDs around the center of the distribution.[34] The decay rate enhancement by the Ag is then a factor 2.1 ± 0.1, and is mostly due to the additional SP decay channel that constitutes 60% of the total decay rate. Experimentally, the decay rate enhancement derived in Sec. III B is 1.8 ± 0.2 at $\lambda=750$ nm. Thus within the error bars good agreement between experiment and theory is observed. The above analysis assumes that nonradiative decay processes do not occur in Si QDs. Including such an effect by the addition to the model of a nonradiative decay rate (W_{nr}), which is not influenced by the presence of the Ag, would bias the calculated decay rate ratio for the SiO_2/air and SiO_2/Ag towards unity. Taking into account the error bars in measurement and calculation, best agreement between experimental and calculated decay rate ratios is achieved when a small $[W_{nr}=(3\pm2)\times10^3\ s^{-1}]$ nonradiative decay rate is included. From the radiative decay rate (extracted from the decay rate measurement and W_{nr}), the SP excitation rate is calculated: $(1.1\pm0.2)\times10^4\ s^{-1}$, which makes Si QDs an ideal candidate for SP excitation. Combining the measured total decay rate (radiative rate W_{rad} plus W_{nr}) and the calculated nonradiative decay rate then leads to a (77 ± 17)% internal emission QE for Si QDs emitting at $\lambda=750$ nm. This is the first direct determination of this quantity and shows the high quality of Si QDs made by ion implantation. The obtained QE is similar to the QE of porous Si nanoparticles,[35] but significantly higher than the QE of Si QDs made in oxidized Si pillars,[18] with both values determined using an indirect method.

Finally, we discuss the large difference in β for the two interfaces, observed in Fig. 4 for the shallowest Si implant. Figure 6 shows that for the shallowest Si implant the decay rates for the SiO_2/Ag interface depend stronger on depth than for the SiO_2/air interface: the variation of decay rate with depth differs by a factor of 5 at the Si peak position. This leads to a larger spread of Si QD decay rates for the SiO_2/Ag interface, and consequently a decrease in β, as is observed.

IV. DISCUSSION

The presented results show that optically active Si QDs can efficiently excite SPs on a SiO_2/Ag interface. For most optimal excitation of SPs the Si QDs should be located at ~40 nm from the SiO_2/Ag interface, where SP coupling is strong and loss processes are relatively small. Coupling to SPs provides a unique way to enhance the effective emission rate and QE of Si QDs. By exciting SPs at a rate W_{SP} and then coupling the SPs out into the far field, the SP excitation that initially constitutes a loss process may be turned into a radiative process.[11,36] In this way the radiative decay rate W_{rad} can be artificially enhanced to $W_{rad}+W_{SP}$. Similarly, for optical emitters with an internal QE<1, coupling to SPs and subsequent out coupling to the far field, can enhance the internal QE. Optimized geometries have shown SP out-coupling efficiencies close to unity.[37]

In the present experiment the SP generation efficiency is 60% for the shallowest Si implant (see Fig. 6), limiting the maximum achievable increase in emission rate and QE. Here we discuss different ways to increase the SP excitation rate. The largest coupling of a dipole to SPs is achieved when the emission frequency matches the SP resonance frequency, i.e., the frequency for which $\varepsilon'_{metal}=-\varepsilon_d$. In the present case, for an emission wavelength of 750 nm, the large discrepancy between the dielectric constant of the SiO_2 ($\varepsilon_{SiO_2}=2.1$) and the Ag ($\varepsilon_{Ag}=-15+i0.86$), results in a relatively small SP coupling rate. Using an alternative host for Si QDs that has a higher dielectric constant will increase the coupling. For example, for a dipole at 44 nm from the interface, emitting at 750 nm with Ag as a metal and Si_3N_4 ($\varepsilon=4$) as a dielectric matrix, 63% of the dipole's excitation energy is converted into SPs.

The SP coupling rate can be further enhanced by modifying the SP dispersion relation by changing the thickness of the metal. For a metal layer with a thickness of the same order of magnitude as the skin depth, SPs propagating at both sides of the metal interact. This results in a splitting of the single SP mode into an asymmetric and symmetric mode.[38] We calculated the thin metal film SP dispersion using Ford and Weber's model. Calculations were performed for a multilayer structure consisting of an optically thick SiO_2 layer on top of a 10 nm thick Ag layer on top of a SiO_2 substrate, with the dipole at 44 nm distance from the Ag layer. The inset in Fig. 7 shows the power dissipation, calculated for a randomly oriented dipole emitting at 480 nm. Clearly, the two SP modes can be observed: the asymmetric SP mode at $k_{\parallel}/k_d=1.0083$, and the symmetric SP mode at $k_{\parallel}/k_d=5.08$. Similar calculations were performed over a large range of frequencies (taking the dispersion of ε_{Ag} into account) and at each frequency the wave vectors of both modes were derived. The result is shown in Fig. 7, with the light line $\omega=kc/\sqrt{\varepsilon_d}$ shown for reference ("light line"). From these data we can observe that, at a given frequency, the wave vector for the symmetric SP mode, in comparison to the infinite Ag layer, is increased and the wave vector for the asymmetric SP mode is decreased. Since the SP mode density is proportional to $d(k^2)/d\omega$,[39] decreasing the film thickness increases the SP mode density for the symmetric SP mode. For the case calculated in Fig. 7, this leads to a tenfold increase in the SP excitation rate. A full calculation of the thin-film SPs excitation rate should also take into account the overlap of the dipole field and the SP mode.

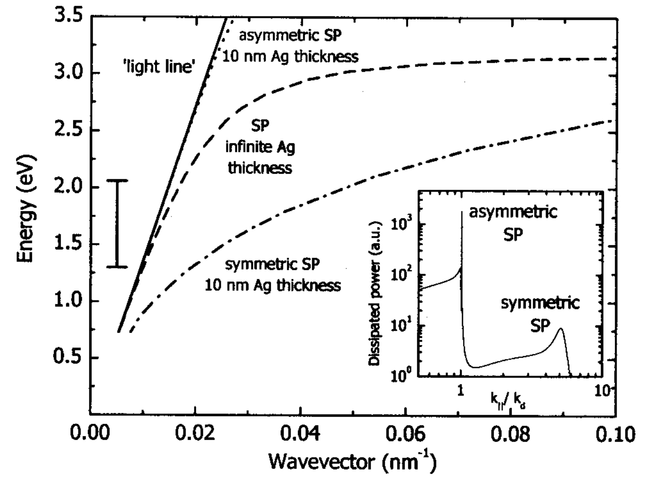

FIG. 7. Dispersion curves for plane wave (solid line) and SP for an infinite Ag thickness (dashed). For a 10 nm thick Ag film embedded in SiO_2 the SP splits into an asymmetric (dotted line) and symmetric mode (dashed-dotted). Inset shows the power dissipation for a randomly oriented dipole embedded in SiO_2, emitting at 480 nm at a distance of 44 nm from the Ag film. Two peaks can be observed: the asymmetric mode at $k_{\parallel}/k_d=1.008$ and the symmetric mode at $k_{\parallel}/k_d=5.09$. The vertical bar indicates the energy range of the Si QD emission.

The present work shows that SP modes can be selectively excited by a strongly coupled dipole, with the symmetric mode being more pronounced for thin films compared to the asymmetric mode. Further work will address this in more detail. Given the fact that Si QDs can be electrically excited,[1,2] coupling to SPs provides a way to electrically generate SPs.

V. CONCLUSIONS

In summary, we have shown that Si QDs can couple to surface plasmons at the Ag/SiO_2 interface, leading to an increase of their decay rate. The average photoluminescence decay rate of Si QDs in SiO_2 is enhanced by 80% when they are placed in close proximity (~40 nm) to a Ag interface. Calculations performed with a classical dipole oscillator model are in good agreement with the data. For the shallowest Si implant the surface plasmon excitation efficiency is 60% and amounts to a surface plasmon excitation rate of $(1.1\pm0.2)\times10^4$ s^{-1}. From a comparison of the experimental decay-rate distributions to the model calculations, we determine the Si QD internal quantum efficiency to be $(77\pm17)\%$. We calculate that the surface plasmon excitation efficiency can be further enhanced by exciting surface plasmons on thin metal films, in which case the symmetric SP mode is preferentially excited. As Si QDs can be electrically excited, this work provides design criteria for an electrically pumped, mode selective, surface plasmon source.

ACKNOWLEDGMENTS

This work was made possible by the fabrication and characterization facilities of the Amsterdam nanoCenter. It is part of the research program of the "Stichting voor Fundamenteel Onderzoek der Materie (FOM)," which is financially supported by the "Nederlandse organisatie voor Wetenschappelijk Onderzoek (NWO)."

*Email address: kalkman@amolf.nl

[1] A. Irrera, D. Pacifici, M. Miritello, G. Franzó, F. Priolo, F. Iacona, D. Sanfilippo, G. Di Stefano, and P. G. Fallica, Appl. Phys. Lett. **81**, 1866 (2002).

[2] J. Valenta, N. Lalic, and J. Linnros, Appl. Phys. Lett. **84**, 1459 (2004).

[3] R. J. Walters, P. G. Kik, D. J. Casperson, H. A. Atwater, R. Lindstedt, M. Giorgi, and G. Bourianoff, Appl. Phys. Lett. **85**, 2622 (2004).

[4] L. Pavesi, L. Dal Negro, C. Mazzoleni, G. Franzó, and F. Priolo, Nature (London) **408**, 440 (2000).

[5] E. M. Purcell, Phys. Rev. **69**, 681 (1946).

[6] R. Sprik, B. A. van Tiggelen, and A. Lagendijk, Europhys. Lett. **35**, 265 (1996).

[7] E. Snoeks, A. Lagendijk, and A. Polman, Phys. Rev. Lett. **74**, 2459 (1995).

[8] T. M. Hensen, M. J. A. de Dood, and A. Polman, J. Appl. Phys. **88**, 5142 (2000).

[9] K. H. Drexhage, J. Lumin. **1–2**, 693 (1970).

[10] W. L. Barnes, J. Mod. Opt. **45**, 661 (1998).

[11] J. Kalkman, C. Strohhöfer, B. Gralak, and A. Polman, Appl. Phys. Lett. **83**, 30 (2003).

[12] J. Zhang, Y.-H. Ye, X. Wang, P. Rochon, and M. Xiao, Phys. Rev. B **72**, 201306(R) (2005).

[13] J. F. Ziegler, J. P. Biersack, and U. Littmark, *The Stopping Range of Ions in Solids* (Pergamon, New York, 1985).

[14] K. S. Min, K. V. Shcheglov, C. M. Yang, H. A. Atwater, M. L. Brongersma, and A. Polman, Appl. Phys. Lett. **69**, 2033 (1996).

[15] M. L. Brongersma, A. Polman, K. S. Min, E. Boer, T. Tambo, and H. A. Atwater, Appl. Phys. Lett. **72**, 2577 (1998).

[16] J. Linnros, N. Lalic, A. Galeckas, and V. Grivickas, J. Appl. Phys. **86**, 6128 (1999).

[17] F. Priolo, G. Franzó, D. Pacifici, V. Vinciguerra, F. Iacona, and A. Irrera, J. Appl. Phys. **89**, 264 (2001).

[18] J. Valenta, R. Juhasz, and J. Linnros, Appl. Phys. Lett. **80**, 1070 (2002).

[19] I. Sychugov, R. Juhasz, J. Valenta, and J. Linnros, Phys. Rev. Lett. **94**, 087405 (2005).

[20] V. Vinciguerra, G. Franzó, F. Priolo, F. Iacona, and C. Spinella, J. Appl. Phys. **87**, 8165 (2000).

[21] B. Garrido Fernandez, M. López, C. Garcia, A. Pérez-Rodriguez, J. R. Morante, C. Bonafos, M. Carrada, and A. Claverie, J. Appl. Phys. **91**, 798 (2002).

[22] A. Thean and J. P. Leburton, Appl. Phys. Lett. **79**, 1030 (2001).

[23] I. Sychugov, R. Juhasz, J. Linnros, and J. Valenta, Phys. Rev. B **71**, 115331 (2005).

[24] E. Helfand, J. Chem. Phys. **78**, 1931 (1983).

[25] G. Mauckner, K. Thonke, T. Baier, T. Walter, and R. Sauer, J. Appl. Phys. **75**, 4167 (1994).

[26] C. P. Lindsey and G. D. Patterson, J. Chem. Phys. **73**, 3348 (1980).

[27] H. Pollard, Bull. Am. Math. Soc. **52**, 908 (1946).

[28] D. Kovalev, H. Heckler, G. Polisski, J. Diener, and F. Koch, Opt. Mater. (Amsterdam, Neth.) **17**, 35 (2001).

[29] C. Garcia, B. Garrido, P. Pellegrino, R. Ferre, J. A. Moreno, J. R. Morante, L. Pavesi, and M. Cazzanelli, Appl. Phys. Lett. **82**, 1595 (2003).

[30] M. V. Wolkin, J. Jorne, P. M. Fauchet, G. Allan, and C. Delerue, Phys. Rev. Lett. **82**, 197 (1999).

[31] G. W. Ford and W. H. Weber, Phys. Rep. **113**, 195 (1984).

[32] W. H. Weber and C. F. Eagen, Opt. Lett. **4**, 236 (1979).

[33] M. J. A. de Dood, L. H. Slooff, A. Moroz, A. van Blaaderen, and A. Polman, Phys. Rev. A **64**, 033807 (2001).

[34] M. L. Brongersma, A. Polman, K. S. Min, and H. A. Atwater, J. Appl. Phys. **86**, 759 (1999).

[35] G. M. Credo, M. D. Mason, and S. K. Buratto, Appl. Phys. Lett. **74**, 1978 (1999).

[36] K. Okamoto, I. Niki, A. Shvartser, Y. Narukawa, T. Mukai, and A. Scherer, Nat. Mater. **3**, 601 (2004).

[37] J. Moreland, A. Adams, and P. K. Hansma, Phys. Rev. B **25**, 2297 (1982).

[38] J. A. Dionne, L. A. Sweatlock, H. A. Atwater, and A. Polman, Phys. Rev. B **72**, 075405 (2005).

[39] I. Gontijo, M. Boroditsky, E. Yablonovitch, S. Keller, U. K. Mishra, and S. P. DenBaars, Phys. Rev. B **60**, 11564 (1999).